26th International Congress on Sound and Vibration
7-11 July 2019, Montreal

UNSTEADY RANS SIMULATION ON THE EFFECT OF FILM COOLING ON ENTROPY NOISE GENERATION IN A TWO-DIMENSIONAL STATOR CASCADE

Thomas Bach, Yasser Mahmoudi and Stephen Spence
School of Mechanical and Aerospace Engineering, Queen's University Belfast, Belfast, UK
email: tbach01@qub.ac.uk

Advances in aero engine technology have reduced jet and fan noise, which has increased the significance of combustion noise and the need to reduce the indirect noise generated by entropy fluctuations as they accelerate through the turbine stages. The present work examines the influence of film cooling on the convection and attenuation of entropy wave as well as the indirect entropy noise generated in a two dimensional stator cascade using an unsteady RANS modelling approach. Initially the mean flow properties of the stator are compared with experimental data from the Politecnico di Milano for an axial turbine stage without film cooling. Afterwards a single film cooling hole is added to the suction side and the pressure side of the stator blade. Results show that the amplitude of the entropy wave reduces due to the secondary flow from the cooling holes. However, the amplitude of the pressure perturbation due to the accelerated entropy wave increases. Both the attenuation of the entropy wave and increasing the amplitude of the generated pressure waves depend on the mass flow rate of the coolant flow.

Keywords: Gas turbine, URANS, Aeroacoustic, Entropy noise, Film cooling

1. Introduction

In the last decade, great efforts have been undertaken to reduce jet, fan and external aerodynamic noise in aircraft, which have left combustion noise as an important remaining contributor [1]. The unsteady combustion process produces direct and indirect noise, where the acceleration of entropy perturbations is the main contributor to indirect noise generation [1]. Though entropy perturbations undergo attenuation effects in the combustor, sufficient strength remains at the combustor exit at low frequencies leading to the generation of entropy noise in the turbine stages [2].

It was Marbel and Candel [3] who first developed an analytical model to predict indirect combustion noise generation for a compact nozzle. However, in a real engine entropy perturbations are not accelerated through a nozzle but through a series of turbine blade rows. Hence Cumpsty and Marble [4] have extended the earlier model, leading to the actuator disk theory assuming a compact blade row where the wavelength of the perturbation is much longer compared to the axial blade cord length. The actuator disk theory has been evaluated with respect to an inviscid two-dimensional (2-D) stator blade row simulation, showing that for planar entropy waves the model predicts the noise generation with an accuracy between 12-38

percent difference, while for more localized entropy disturbances the discrepancies are much larger [5]. To improve upon the actuator disk theory, a low-order model solver (called LINEARB [6]) was developed based on the semi-actuator disk model not relying on the compact theory anymore but still disregarding entropy wave attenuation, which improved the combustion noise prediction at turbine exit [6]. In an attempt to predict the combustion noise at turbine exit of the Rolls-Royce ANTLE aero-engine, the level of combustion noise has been over-predicted by almost two order of magnitude [6]. Mahmoudi et al. [6] discussed that the main reason for such high over-prediction is attributed to the effect of the attenuation and dissipation of entropy waves in real engines which were not considered in their low order model.

To improve analytical models and better understand the convection and attenuation of entropy waves, the transport of entropy perturbations have been studied in a duct [7] and pipe flow [8]. It was found that in such simple geometries, shear dispersion due to the mean velocity profile is the main reason for the attenuation of entropy waves. Turbulent mixing and diffusion may also contribute to the entropy wave attenuation at high frequencies and increasing residence time [8]. Using a 2-D large-eddy simulation (LES) Leyko et al. [9] showed that entropy waves are attenuated through a stator blade passage due to shear dispersion, non-uniform velocity profile . This effect was more significant for wave lengths smaller than the blade passage length. While large wave lengths were less attenuated and reach the outlet of the domain almost unchanged [9]. Therefore the actuator disk theory predicts the transmission and reflection of an acoustic wave due to an entropy incident wave reasonably well if the wave length, λ, is 10 times larger than the axial cord length (C_{ax}) of the blade row i.e. $\lambda/C_{ax} > 10$ [9]. The same is true for the transmission and reflection of an acoustic incident wave [9]. This analytical model accounting for entropy wave attenuation due to the deformation caused by the mean axial velocity profile was extended to an entire turbine stage [10]. A 2-D LES model is limited in predicting the turbulent mixing as the large vortical structures cannot develop at the trailing edge [10]. Therefore the entropy wave attenuation has been evaluated in a transonic 3-D LES simulation, with a forced planar entropy wave of 2000 Hz corresponding to the limit of the validity of the compact theory found in previous 2-D simulations [11]. This revealed an even stronger entropy wave attenuation compared to the 2-D results by Bauerheim et al. [10], while the acoustic wave transmission stayed roughly the same between 2-D and 3-D simulations. However a small reduction in the acoustic wave reflection occurs between the two cases, possibly due to the chocked flow of the transonic operating condition [11].

Further turbine details have been investigated such as the effect on indirect noise in the presence of a shock. This was done within an LES approach of a 3-D nozzle guide vane section at transonic operating conditions where a weak normal shock was present [12]. This showed that additional pressure fluctuations were emitted in the area of the shock due to the interaction of the shock with the forced entropy wave [12]. However these pressure fluctuations generated downstream of the sonic throat cannot travel upstream [12]. Previous work modelled the entropy wave as a planar wave, while entropy fluctuations are more locally concentrated at combustor exit [5, 9, 10, 11, 12]. Therefore local entropy wave streaks were investigated in comparison to planar entropy waves. The 3-D LES simulation of Becerril et al. [13] showed that over the stator, the amplitude of the entropy wave streak was very little attenuated as it acts as a passive scalar following the streamlines and was not deformed as much as a planar entropy wave [13]. Nevertheless, higher frequencies get more attenuated as the dispersion effect on the entropy wave streak is higher compared to low frequencies [7, 8, 13]. When the entropy wave streak passes through the rotor, the waves are attenuated due to the mixing promoted by the rotational velocity of the rotor, secondary flows and shock waves [12, 13]. The entropy noise generation is most important in the first turbine stage as entropy fluctuation are only weakly transmitted to consecutive turbine stages [11].

Entropy fluctuation are not only very localised but are also located within a very hot mean flow, reaching turbine entry temperatures (TET) above 1800K in modern aero engines. This requires very sophisticated turbine cooling systems, such as film cooling, in order to keep the turbine blades at safe

operating conditions [14]. Through the discrete film cooling holes bleed air from the compressor is ejected creating a protective layer of cool air around the turbine blade. The effect of such a cooling flow on an incoming localized entropy perturbation was investigated experimentally in a convergent-divergent nozzle, where air at ambient temperature was injected through a perforated liner located upstream of the nozzle [15]. This showed that the strength of the entropy wave was reduced by 3-6% and a reduction in the indirect entropy noise was observed downstream of the nozzle [15]. Though the effects of the secondary flow depend on the operating condition of the test rig, it showed that a cooling flow can have an attenuation effect on an incoming entropy wave as well as the entropy noise generated. The present work examines the effect of the cooling flow on the convection and associated noise generated of an entropy wave in a 2-D stator blade in a frequency range of 200 Hz to 1000 Hz [1] by solving the Unsteady Reynolds-Averaged Navier-Stokes (URANS) equations. Though similar studies have been completed for a stator blade by various authors making different assumptions (e.g. 2-D geometry, inviscid, planar entropy wave, no cooling) [5, 9, 16], this study incorporates a simplistic 2-D film cooling model into a stator blade with a cooling flow on the suction surface and pressure surface, with its effect on indirect noise yet unknown.

2. Numerical model

For this study the stator geometry with 22 blades from the high pressure turbine at the Politecnico di Milano has been used, with experimental data published by Knobloch et al. [17]. As this blade geometry does not contain any film cooling geometry, a similar configuration has been applied as presented by Bassi et al. [18] modelling a single hole on the pressure surface (PS) and suction surface (SS) with a hole diameter of 0.5 mm. Due to the 2-D assumption the model is representative of a film cooling slot rather than a discrete hole. The 2-D stator profile has been extracted at mid-span of the blade, modelling a single blade passage corresponding to 16.4 degree of the annulus. The stator domain with its boundary conditions (BC) are shown in Fig. 1. Periodic BC have been applied modelling a stator cascade (Fig. 1). The outlet was specified as an opening with a static pressure (106.7 kPa) to allow an acoustic non-reflective BC. At the inlet the normal velocity (43.5 m/s) and the total temperature (T_{tot}) of 323 K were specified, without any initial turbulent intensity to avoid indirect noise due to vorticity fluctuations. The velocity inlet was of importance for the forced case, to suppress the pressure wave introduced by the unsteady temperature signal (direct noise) which was modelled as a sinusoidal wave,

$$T_{tot} = \overline{T}_{tot} + \Delta T \times \sin(2\pi f), \tag{1}$$

where f is the frequency. As non-reflective BC was not possible at the inlet and outlet, an extended domain (twice the acoustic wavelength of the lowest frequency considered) with a reflective BC is considered at the inlet. This length is required to make sure that when the upstream travelling pressure waves (generated by the interaction of the entropy wave with the stator blade) reflected from the upstream boundary, do not reach the stator blade. This inlet design enables the separation of the upstream travelling pressure waves due to the entropy forcing and reflected pressure waves from the inlet. In the case of film cooling, also shown in Fig. 1, all BC were kept the same but a mass flow rate and total temperature was specified at the SS and PS inlet. A grid independence study on the pressure and entropy transfer functions (TF) has been carried out on a coarse, medium and fine mesh with 201 k, 433 k and 997 k elements respectively. The difference between the TFs of the medium and fine mesh was less than less than 0.8%. Hence, the medium size mesh was chosen to produce the results presented in this paper. The Y^+ value on the blade surface is ≈ 1. Additionally, time independence was checked with a time step of 2×10^{-5}s, 1.33×10^{-5}s and 0.8×10^{-5}s. The percentage change between the TFs with a time step of 2×10^{-5}s and 1.33×10^{-5}s was less than 1%. Hence, the time step 2×10^{-5}s was chosen for this work.

ANSYS CFX 18.2 has been used to solve the URANS equations within the 2-D stator domain, as also utilised by others to evaluate the acoustic field in radial compressors [19]. To account for the Reynold stress term in the mean flow the SST-turbulence model [19] has been used. The advection scheme and turbulence numerics were set to high resolution making use of the second order backwards Euler scheme, also used by the transient scheme. Air was modelled using the ideal gas law (constant c_p).

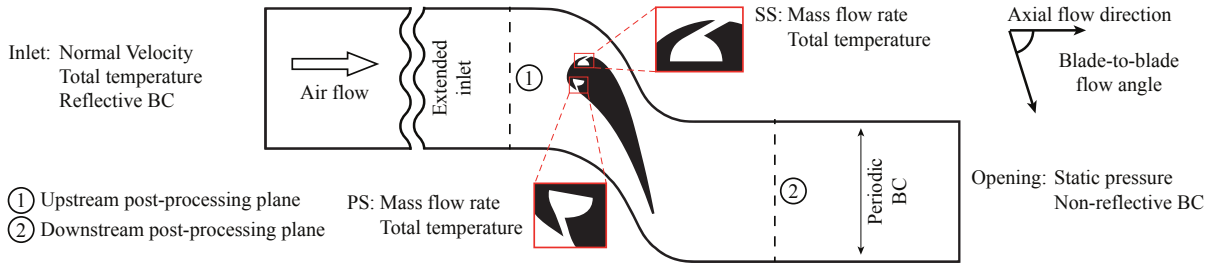

Figure 1: Stator domain with boundary conditions and film cooling detail on the PS and SS.

3. Results

3.1 Aerodynamics

The mean flow field without film cooling was validated with respect to the experimental data of Knobloch et al. [17]. Downstream of the stator, circumferential averaged data for the pressure ratio $P/P_{tot,ref}$ ($P_{tot,ref}$ = total pressure at inlet), Mach number and the blade-to-blade flow angle (Fig. 1) at $x/C_{\text{ax}} = 1.32$ from the stator leading edge are obtained and compared with the experimental data. The results are shown in Fig. 2 with the respective errors. Good agreement was found between the present 2-D results against the experimental data of Knobloch et al. [17]. An under-prediction of -4.9% was observed for the upstream Mach number and an overestimation of 4.7% was found for the downstream Mach number. Such discrepancy may be attributed to the 2-D assumption disregarding any spanwise flow.

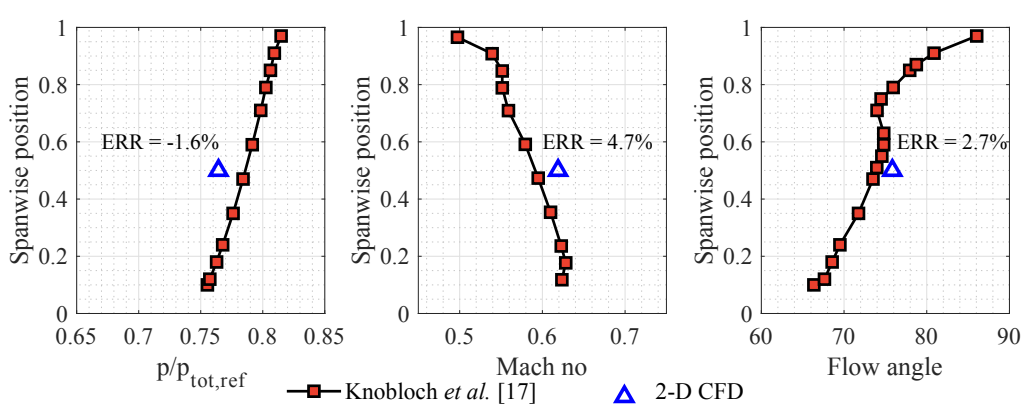

Figure 2: Aerodynamic validation at $x/C_{\text{ax}} = 1.32$ downstream from the stator leading edge [17].

For comparison the inlet BC were kept the same for the two cases , i.e. the simulation reference case (no film cooling) and the initial case with film cooling. The film cooling parameters such as density ratio ($DR = \rho_c/\rho_\infty$), blowing ratio ($M = \rho_c U_c/\rho_\infty U_\infty$) and momentum flux ratio ($I = \rho_c U_c^2/\rho_\infty U_\infty^2$) have been closely matched to experimental data of Bassi et al. [18], where the subscript c stands for the coolant

flow and ∞ for the mainstream quantities measured at the inlet. Since the main objective of this work is to analyse the effect of the film cooling on the entropy noise generated, the film cooling mass flow rate were changes in the simulation in the range of [0.9-8.1]$\times 10^{-5}$kg/s, which will change the momentum flux and blowing ratio.

3.2 Acoustics

The unsteady flow field was solved for forced entropy wave frequencies (Eq. 1) between 200 Hz to 1000 Hz corresponding to entropy wave lengths of 7.5-1.5 times the axial cord length (λ/C_{ax}), falling below the limit of the compact theory [9]. The pressure and entropy waves were evaluated as proposed by Marble and Candel [3] shown in Eqs. (2) and (3) respectively, where $A^{\pm}$ represent the normalised amplitudes of the upstream and downstream travelling pressure waves. σ stands for the normalized entropy s, where p is the static pressure, ρ is the density, u is the axial flow velocity and c is the speed of sound. c_p is the specific heat at constant pressure and γ is the ratio of specific heat. The primed quantities refer to the perturbations while the mean quantities are indicated by the bar.

$$A^{\pm} = \frac{p'^{\pm}}{\gamma\overline{p}} = \frac{1}{2}\left[\frac{p'}{\gamma\overline{p}} \pm \frac{u'}{c}\right] \tag{2}$$

$$\sigma = \frac{s'}{c_p} = \frac{p'}{\gamma\overline{p}} - \frac{\rho'}{\overline{\rho}} \tag{3}$$

To evaluate how the pressure responds to an incoming entropy wave and entropy wave attenuation, transfer functions (TF) were evaluated at $x/C_{\text{ax}} = -0.65$ upstream and $x/C_{\text{ax}} = 2.40$ downstream of the stator leading edge, plane 1 and 2 in Fig. 1 respectively. The area averaged static pressure and mass averaged density, static temperature and velocity components were extracted to calculate the pressure and entropy wave strength. The Fast Fourier Transform (FFT) method was used to convert the signals from the time domain into the frequency domain, selecting a period time of 0.01s to achieve a frequency resolution of 100 Hz. The different TFs were then evaluated between plane 1 and plane 2, where the entropy TF $[\sigma_2/\sigma_1]$ gives an indication of entropy wave attenuation, $[p_1^-/\sigma_1]$ and $[p_2^+/\sigma_1]$ show the reflected and transmitted acoustic wave signal.

The generation of indirect noise as the entropy wave passes through the blade is illustrated in Fig. 3 for the reference case (no film cooling) at a forced frequency of 1000 Hz. This shows the entropy wave before reaching the stator at ($t = 0.0855$s) where no pressure perturbation are present upstream of the stator and downstream they are of negligible magnitude. As the entropy wave enters the blade domain ($t = 0.0868$s) and convects downstream with the mean flow, pressure perturbations are generated travelling upstream and downstream, while the entropy waves are being distorted due to the mean velocity profile. The TFs obtained by the present URANS model for the reference case are shown in Fig. 3 (right). In order to understand the effect of diffusion on the generation of the entropy noise, the results of the Euler simulations are plotted in Fig. 3. Additionally, the results of a computational aeroacoustics (CAA) model based on linearised Euler simulations by Emmanuelli et al. [16] are also shown in Fig. 3. When comparing the URANS and Euler results, the entropy wave TF is over-predicted, as the effect of diffusion is not considered in Euler simulations. In comparison to the Euler results, the acoustic TFs are higher for the URANS simulation. This is attributed to the viscous effect near the stator wall, which causes formation of the boundary layer and hence a gradient in the mean flow velocity. Such gradient leads to a higher flow acceleration and hence higher indirect entropy noise. The differences between the CAA [16] and the present Euler results can be due to the different mean velocity field, since the inlet and outlet Mach numbers were under-/overestimated respectively, leading to greater acceleration in the present Euler simulation.

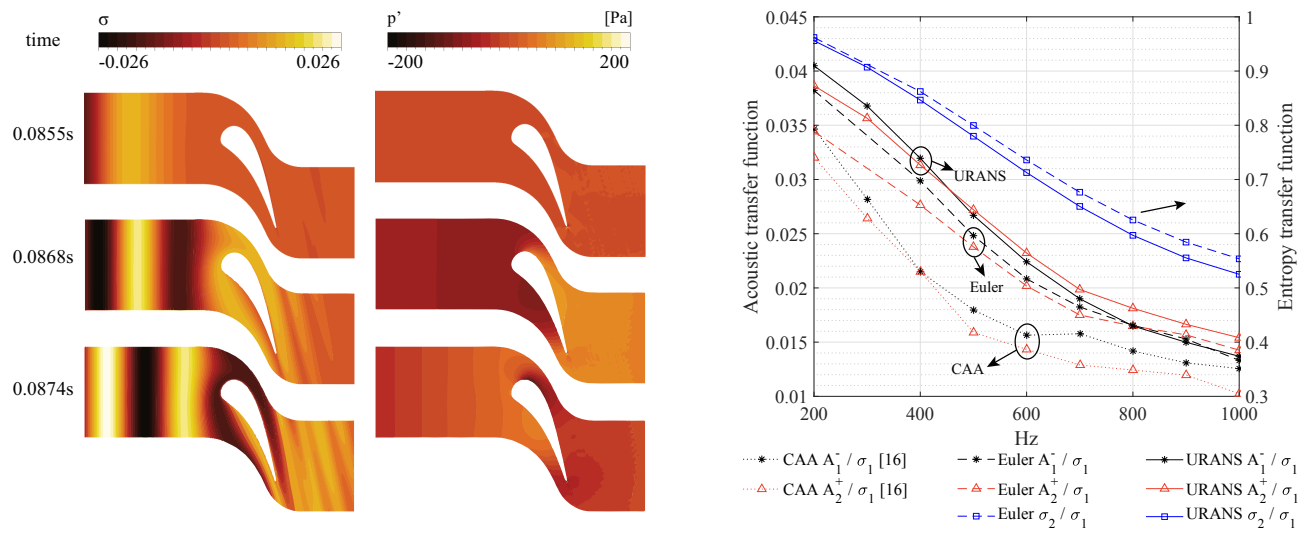

Figure 3: Entropy noise generation at 1 kHz for the reference case (left) and reference TFs from 200Hz to 1kHz (right) for Euler and URANS with CAA results by Emmanuelli et al. [16] for the acoustic TFs.

In order to investigate the impact of film cooling on entropy noise generation, the case without film cooling was considered as a reference case and the impact of film cooling is reported in terms of a percentage difference from the reference case (i.e. Difference = (TF_{film} - TF_{ref}) / TF_{ref}). The percentage difference in TF for film cooling is shown in Fig. 4 for $[\sigma_2/\sigma_1]$ (left), $[A_1^-/\sigma_1]$ (middle) and $[A_2^+/\sigma_1]$ (right). Three different cases were compared changing the mass flow rate of injected cooling flow on the SS while the PS was kept unchanged. The mass flow rate was raised from 0.9×10^{-5} kg/s (case 1) to 2.7×10^{-5} kg/s (case 2) and 8.1×10^{-5} kg/s (case 3). In all cases the film cooling flow stayed attached to the blade and did not separate.

Looking at the entropy wave TF $[\sigma_2/\sigma_1]$, a weak attenuation effect is apparent with a difference of approximately -1.55%, -2.16% and -3.72% for cases 1-3 respectively, which can be attributed to the total film cooling mass flow rate increase of 1.50%, 2.03% and 3.62% of the mean inlet mass flow rate. A greater attenuation may have been expected, however as the film cooling flow stays attached to the blade limited mixing occurs. Additionally, the turbulence intensity in the domain stays below 1% as no initial turbulent intensity was introduced at the inlet, preventing further attenuation due to the mixing. The attenuation effect due to shear dispersion was also very limited as the film cooling flow only changed the velocity profile in the vicinity of the boundary layer of the blade. Nevertheless, considering the underlying physics, the results are within the expected range in comparison to an earlier experiment with a bias flow liner in front of a nozzle [15].

Though the entropy wave strength has been slightly attenuated, the amplitudes of the reflected and transmitted pressure waves associated with the entropy wave increased (Fig. 4). A maximum difference appears at a frequency of 700 Hz, before the impact of film cooling decreases again. The reason for this is currently unknown and the physics behind such a behaviour requires further investigation. However the general increase can be explained by the increase in mass flow rate through the blade passage due to film cooling. This increased the velocity of the perturbed flow, hence the convective acceleration within the stator flow field changed, leading to a change in pressure perturbation according to Marble and Candel [3]. The change of acceleration was visualised in Fig. 5 (left) by subtracting the reference case from the film cooling case along with the change in pressure perturbation (right). This shows that the acceleration changes locally where the flow was injected as well as in the throat region of the blade passage. The local acceleration on the PS did not have a significant effect on the pressure perturbation Fig. 5. However the

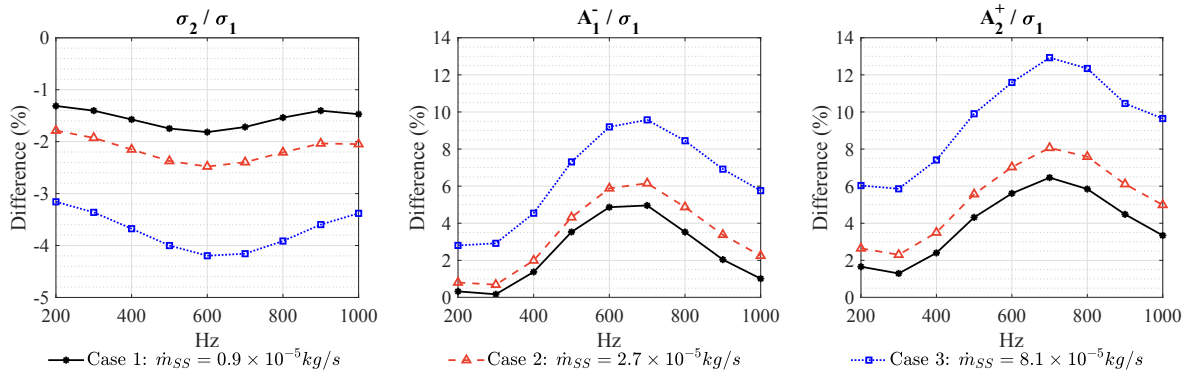

Figure 4: Percentage difference in transfer function (TF) between the film cooling cases 1-3 and the reference case, Difference = (TF_{film} - TF_{ref}) / TF_{ref}.

local acceleration on the SS contributes towards the change in pressure perturbation. Yet, the greatest change was observed in the throat of the blade passage as the entire entropy wave was accelerated.

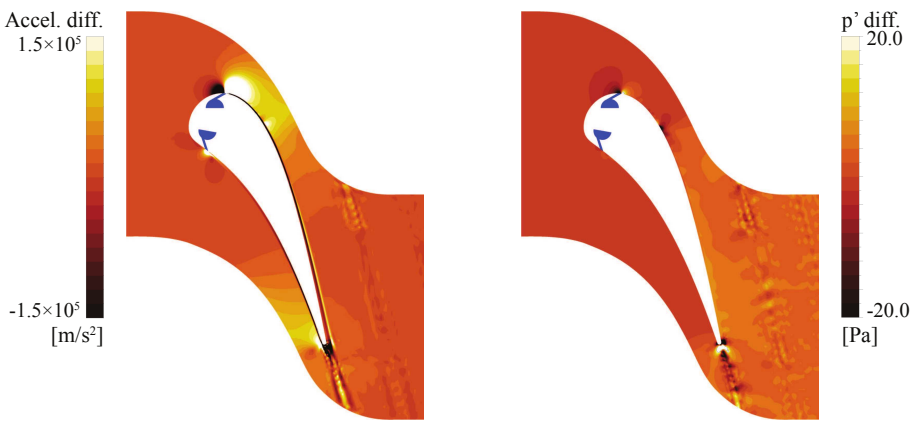

Figure 5: Convective acceleration (left) and pressure perturbation (right) difference between the reference case and case two at 700 Hz.

4. Conclusion

The present study examined the effect of film cooling in a turbine stator blade row on the generation of indirect entropy noise. 2-D unsteady RANS computations were performed for a wide range of film cooling mass flow rates. Results show that the entropy waves were slightly attenuated by the film cooling flow. As the entropy waves convect through the blade passage, the film cooling flow changes the flow acceleration within the passage resulting in additional entropy noise. Comparison between a URANS and Euler simulation also showed that neglecting viscosity and thermal diffusion leads to an over-prediction in entropy transfer function. However, since Euler simulations disregard the formation of the boundary layer, it under-predicts flow acceleration and hence lower entropy noise.

5. Acknowledgement

The author would like to thank Prof. P. Geatani from the Politecnico di Milano for making the geometry of the high pressure turbine available to us. This work was supported by the Engineering and

Physical Sciences Research Council (EPSRC).

REFERENCES

1. Dowling, A.P. and Mahmoudi, Y. Combustion noise. *Proceedings of the Combustion Institute*, **35** (1), 65–100, (2015).
2. Xia, Y., Duran, I., Morgans, A.S. and Han, X. Dispersion of entropy perturbations transporting through an industrial gas turbine combustor, *Flow, Turbulence and Combustion*, **100** (2), 481–502, (2018).
3. Marble, F. E. and Candel, S. M., Acoustic disturbance from gas non-uniformities convected through a nozzle, *Journal of Sound and Vibration*, **55** (2), 225–243, (1977).
4. Cumpsty, N. A. and Marble, F. E., The interaction of entropy fluctuations with turbine blade rows; a mechanism of turbojet engine noise, *Proc. R. Soc. Lond. A*, **357**, 323–344, (1977).
5. Mishra, A. and Bodony, D. J. Evaluation of actuator disk theory for predicting indirect combustion noise, *Journal of Sound and Vibration*, **332**, 821–838, (2013).
6. Mahmoudi, Y., Guisti, A., Mastorakos, E. and Dowling, A.P. Low-order modelling of combustion noise in an aero-engine: The effect of entropy dispersion, *Journal of Engineering for Gas Turbines and Power*, **140** (1), 011502, (2018).
7. Morgans, A.S., Goh, C.S. and Dahan, J.A. The dissipation and shear dispersion of entropy waves in combustor thermoacoustics. *Journal of Fluid Mechanics*, **733** (R2), (2013)
8. Giusti, A., Worth, N.A., Mastorakos, E. and Dowling, A.P. Experimental and numerical investigation into the propagation of entropy waves. *AIAA Journal*, **55** (2), 446–458, (2016)
9. Leyko, M., Duran, I., Moreau, S,. Nicoud, F. and Poinsot, T. Simulation and modelling of the waves transmission and generation in a stator blade row in a combustion-noise framework, *Journal of Sound and Vibration*, **333**, 6090–6106, (2014).
10. Bauerheim, M., Duran, I., Livebardon, T., Wang, G., Moreau, S. and Poinsot, T. Transmission and reflection of acoustic and entropy waves through a stator-rotor stage, *Journal of Sound and Vibration*, **374**, 260–278, (2016).
11. Papadogiannis, D., Wang, G., Moreau, S., Duchaine, F., Gicquel, L. and Nicoud, F. Assessment of the indirect combustion noise generated in a transonic high-pressure turbine stage, *Journal of Engineering for Gas Turbines and Power*, **138** (4), 041503, (2015).
12. Ceci, A., Gojon, R. and Mihaescu, M., Large eddy simulations for indirect combustion noise assessment in a nozzle guide vane passage, *Flow, Turbulence and Combustion*, 1–13, (2018).
13. Becerril, C., Moreau, S. and Gicquel. L.Y.M. Study of combustion noise generation in a realistic turbine stage configuration, *GT2018-75062*, Oslo, Norway, 11–15 June, (2018).
14. Xu, L., Bo, S., Hongde, Y. and Lei, W. Evolution of Rolls-Royce air-cooled turbine blades and feature analysis, *Procedia Engineering*, **99**, 1482–1491, (2015).
15. Knobloch, K., Werner, T. and Bake, F. Entropy noise generation and reduction in a heated nozzle flow, *2015 AIAA/CEAS Aeroacoustics Conference*, Dallas, Texas, 22–26 June, (2015).
16. Emmanuelli, A., Huet, M., Le Garrec, T. and Ducrix, S. Study of entropy noise through a 2D stator using CAA, *2018 AIAA/CEAS Aeroacoustics Conference*, Atlanta, Georgia, 25–29 June, (2018).
17. Knobloch, K.,Neuhaus, L., Bake, F., Gaetani, P. and Persico, G. Experimental assessment of noise generation and transmission in a high-pressure transonic turbine stage, *Journal of Turbomachinery*, **139**, 101006, (2017).
18. Bassi, F., Fontaneto, F., Franchina, N., Ghidoni, A. and Savini, M. Turbine vane film cooling: Heat transfer evaluation using high-order discontinuous Galerkin RANS computations. *International Journal of Heat and Fluid Flow*, **61**, 610–625, (2016).
19. Menter, F.R. Two-equation eddy-viscosity turbulence models for engineering applications, *AIAA journal*, **32** (8), 1598–1605, (1994).
20. Banica, M.C., Limacher, P., Feld, H.J. and Spinder, C. Numerical prediction of the sources and the modal content of the acoustic field in a radial compressor outflow, *Journal of Engineering for Gas Turbines and Power*, **139** (9), 092605, (2017).